Mobile Robots with Novel Environmental Sensors for Inspection of Disaster Sites with Low Visibility

Project start: January 1, 2015

Duration: 3.5 years

Deliverable 4.2

Software Toolkit - Hazard prediction based on multimodal perception

Due date: month 40 (April 2018)

Lead beneficiary: LUH

Dissemination Level: PUBLIC

Main Authors:

Paul Fritsche (PF, LUH), Björn Zeise (BZ, LUH), Patrick Hemme (PH, LUH)

Version History:

0.1: Initial version, BZ, March 2018

0.2: Updated version, PF, April 2018

0.3: Corrected version, PF, June 2018

Content

Abstract

This document is a technical report within the scope of the Horizon 2020 project SmokeBot. SmokeBot's objective is to improve the application of mobile robots in disaster scenarios with low visibility conditions. A key element of the project is to develop perception algorithms that support the cooperation of humans and machines in search and rescue missions. This is done with the aid of a novel, multimodal sensor unit, which combines radar, gas, thermal and traditional vision sensors.

This report summarizes the results of Task 4.2 ("Detection and Prediction of Hazards"). Task 4.2 is part of Work Package 4 ("Situation Analysis"), which aims at robustly analyzing the current situation and predicting future progression. This is done by interpreting the data originating from the different information sources available on the robot. The objective of Task 4.2 in particular is to develop a software toolkit that supports humans in fast and reliable situation analysis. This includes algorithms for the complex interpretation of sensor sources in order to detect and predict hazards.

1. Introduction and Purpose of this Document

SmokeBot aims at supporting first responders in situations that are too dangerous for human personnel. Using a robot equipped with a wide range of heterogeneous sensors can be of benefit to the rescue forces and the robot itself when it comes to self-preservation. In order to accomplish tasks such as hazard detection and mapping, all the information provided by the sensors needs to be processed and stored in a meaningful way using an information model. SmokeBot's information model, which is called GDIM (general disaster information model), is described in D4.1 ("Technical specifications for multi-layered information storage model").

This report covers the task of hazard detection and prediction. We present software methods providing functionalities such as threshold-based hazard detection, generation of maps containing different modalities (e.g. temperature, smoke), and hazard prediction (investigation of pre-flashover conditions and modelling of gas, thermal and smoke distribution).

The report is organized as follows:

- Section 2 presents the classification into low and high level hazards
- Section 3 presents the software toolkit for hazard prediction
- Section 3.1 presents low level hazard detection software toolkit
- Section 3.2 presents generation of modality maps
- Section 3.3 presents high level hazard prediction in case of flashovers
- Section 3.3 presents high level hazard prediction for gases, smoke and temperature
- Section 4 presents results from experiments

2. Types of Hazards

Before developing hazard prediction methods, we classified different kinds of hazards after talking to firefighters of the fire department of Dortmund. We realized that we can detect some hazards directly from sensor data. On the other site, a hazard can happen in the future and needs to be predicted with a model. Therefore, we distinguish between low-level and high-level hazards

- Low-level hazards: detection (directly evaluating sensor data)
- High-level hazards: prediction (combining several low-level modalities in order to infer a high-level hazars)

2.1 Low-level Hazards

In the detection part of the framework, a hazard's change over time will not be investigated. Instead, the detection of hazards will be realized by analyzing current (synchronized) sensor data individually. The result of hazard detection are low-level hazards as depicted in Table 1.

Table 1: Low-level hazards

Hazard Category	**Hazard**	**Description**	**Sensor Information**
High temperature	Remotely detected hot spot	Heat sources detected by the robot from a distance using 3D temperature mapping (Task 3.2).	- Thermal images - 3D perception (Lidar, radar, thermal stereo vision)
	High ambient temperature	Temperatures measured in the robot's immediate proximity using on-board temperature sensors.	- On-board temperature sensor - Robot position in map
Gas-related	Remotely detected low visibility	Low visibility due to smoke, fog, mist or dust remotely detected based on the laser radar ratio.	- 3D/2D perception (laser radar ratio)
	Low visibility based on gas measurements	Low visibility due to smoke, fog, mist or dust detected in the robot's immediate proximity by using gas sensor data and the robot's current position.	- Gas sensor - Robot position in map
	Harmful gases	Harmful and toxic gases detected by the gas sensor.	- Gas sensor - Robot position in map
Communication problem	Wi-Fi dead spot	Communication loss due to Wi-Fi dead spots/zones can be identified using watchdog information (continuously pinging the network adapters).	- Watchdog information - Robot position in map

2.2 High-level Hazards

In contrast to these low-level hazards, the hazard prediction procedure will output high-level hazards that represent combinations of low-level hazards and their change over time. To accomplish hazard prediction, a map containing all recognized hazards is needed. This map will be evaluated over time in order to generate a prediction of possible future hazards. Table 2 shows some high-level hazards that may be relevant to the SmokeBot scenario.

Table 2: High-level hazards

Hazard	Indications	Description
Explosion	- Heat - Flammable gas	Rapid combustion of flammable gas as a result of ignition due to a heat source
Flashover [1, 2]	- Temperature of approx. 600 °C under the ceiling - Pulsating smoke coming out of a room - Heat flux at floor level	Transition between fire development and full fire
Backdraft [2]	- Little/no ventilation (lack of oxygen) - Hot fuel gases and smoke	Combustion in a room with no ventilation will create hot combustible fuel gases and smoke. Due to the lack of oxygen, the gas/smoke mixture is not able to ignite although having a temperature above self-ignition temperature. Reintroducing oxygen (e.g. by opening a window/door) will lead to a rapid combustion.
Rollover [2]	- Flammable gases - Ignition source	Ignition of flammable gases located under the ceiling of a room

The detection and prediction of the above-mentioned high-level hazards is not trivial. Their occurrence depends on many (unknown) factors (e.g. geometry of the regarded building, building interior, type of fire, etc.) and is therefore badly predictable. Nevertheless, some of the typical indications can be detected using the robot's sensing capabilities.

3. Software Toolkit

3.1 Low-level Hazard Detectors

As a first step towards hazard detection, we decided to develop independently working hazard detectors that generate hazard features. Hazard features consist of information like hazard type, intensity, location and area. According to the low-level hazards listed in Table 1, the following hazard detectors have been developed:

Communication Monitor

The monitoring tool of GDIM is a tool that monitors the WiFi's signal strength. In case the signal strength value drops below a certain threshold, a hazard feature containing the information about connection loss is published and indicated to the operator through the visualization.

Ambient Temperature Monitor

The monitoring tool of GDIM observes the robot's temperature, i.e. the temperature at the robot's current position. This information can be obtained from several sources in the SmokeBot system, since almost every of the sensors measures the on-board temperature. If the temperature passes a certain threshold, a warning is indicated to the operator through the interface.

Hotspot Detector

Using the information provided by the laser/radar scanner and the thermal imaging camera, hotspots in the robot's field of view are remotely detected. For this purpose, the temperature mapping software toolkit (D3.2) is used to obtain a tempered point cloud or laser scan, respectively. By performing spatially and temperature-based clustering, potential hotspots in the environment can be identified and published.

Internal Hazards

The Smokebot tracker is a complex system, where internal problems can occur. For example overheated CPU, Software crashes, communication problems or hardware damages are some examples. The operator gets informed over the systems health through the interface.

Hazard Visualization

All hazards are given to the operator through the visualization. (see Fig. 1).

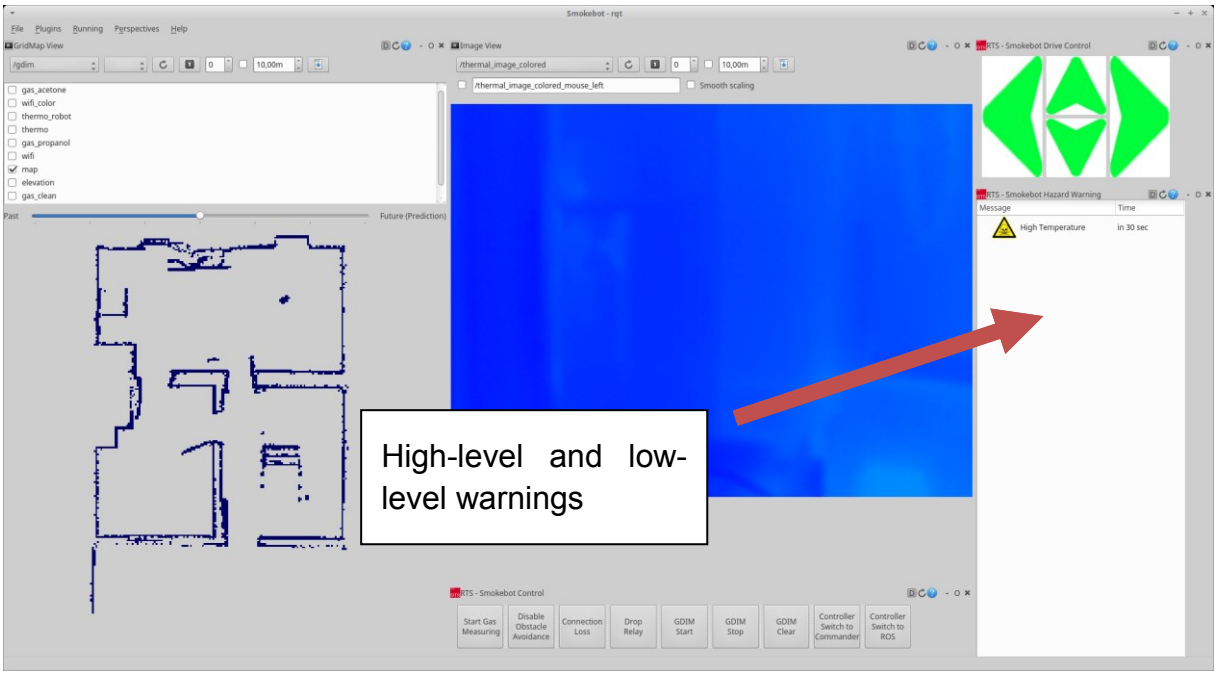

Fig. 1: Graphical user interface displaying low-level and high-level hazards as warning in a list

3.2 Generation of Map Layers with Different Modalities

As an input for the hazard mapping task (T4.3), a set of multi-modal submaps that is linked via geometric transformations provided by the SLAM algorithm is generated. This procedure was already described in detail in D4.1 (“GDIM”). For this reason, we only give a short explanation on this topic here.

Submaps depict partial views of the environment. Each submap is generated using the sensor data available during a certain route segment while the robot travels through the scenario. Several submaps are linked to each other using transformations that are published by the graph-based SLAM (D1.8). Using the submaps and the transformations, GDIm stitches together a global map.

The advantage of using submaps is that the global maps can even be corrected if there is a change in the environment by using updated transformations. This is especially useful if the robot visits places that it has seen before (also called *loop closure*).

The implementation of the (sub-)mapping processes is based on the grid_map package [4]. Submaps of different modalities are saved in one grid map. Each modality has an individual layer in this grid map. The layers (modalities) used in SmokeBot are:

- Remote temperature (i.e. measured at a certain distance using range sensors and thermal imaging)
- Smoke (determined using the laser-radar-ratio method, see D1.7)
- Signal strength
- Acetone concentration (Using gas sensing unit of UWAR)

- Propanol concentration (Using gas sensing unit of UWAR)

3.3 High Level Hazards: Flashover Prediction

A flashover is a spontaneous combustion, which can occur at furniture or doors due to the release of flammable gases when certain organic materials are heated. A flashover happens usually around 500 °C. Before a flashover occurs, smoke is usually spread across the ceiling in the room. Due to the rising smoke, a lot of heat is gathering at the ceiling as well. Therefore, doors or similar objects show a temperature gradient (see Fig. 2).

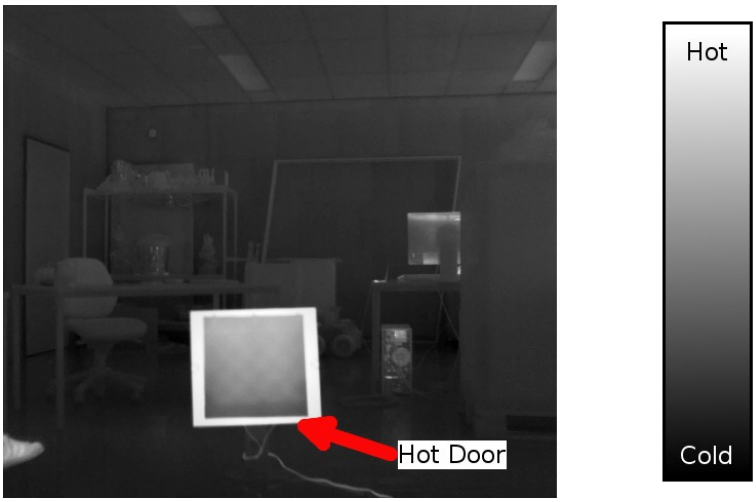

Fig. 2 This thermal image is representing a hot object showing a temperature gradient.

To sum it up, in order to detect a possible flashover, an object needs to show a temperature gradient and rising smoke. An object representing a cause of a flashover is depicted in Fig. 2. In order to detect a flasover, the object needs to be extracted from the thermal camera image. Then, the object needs to be analyzed regarding an existing temperature gradient. If an at least 500°C hot object shows a temperature gradient and causing smoke, then it is a warning for likely flashovers. The process of a flashover detection strategy in case of a door is show in Fig. 3.

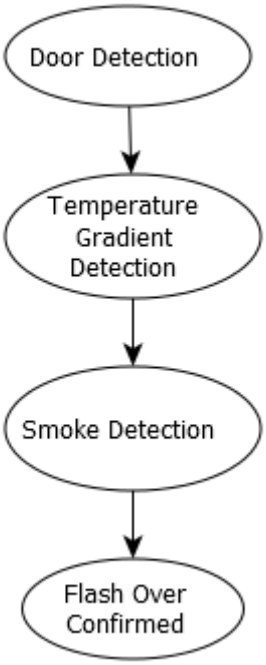

Fig. 3 Flashover detection procedure in case of a door (Object detection, temperature gradient detection and smoke detection)

3.3.1 Object Detection

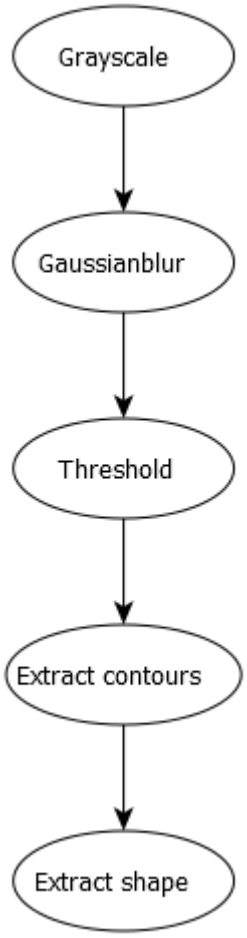

Flashovers occur mostly at doors. Doors come in different variations and colors, but all doors are rectangular, which can be detected through contour extractions. With the contours detected, a approximated polygon can be calculated. Every polygon is broken down to its corners, leaving rectangular objects in the scene.

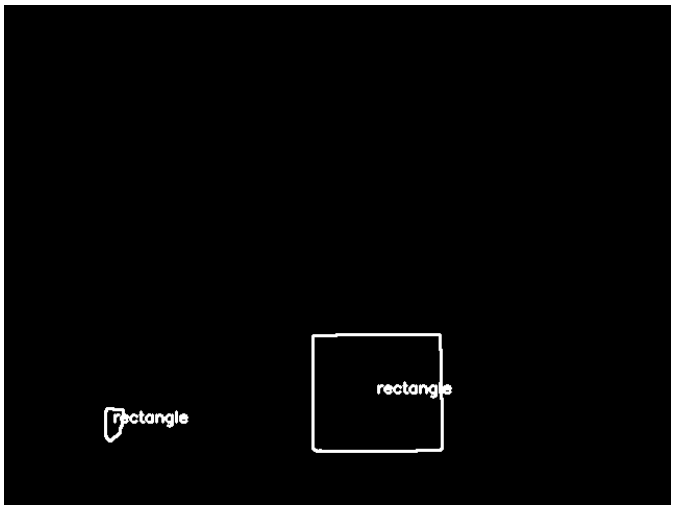

Fig. 4
Left: Detection procedure
Above: Detecting rectangular objects as for example doors.

3.3.2 Temperature Gradient Detection

At first, a temperature gradient needs to be detected vertically along the surface of an object.

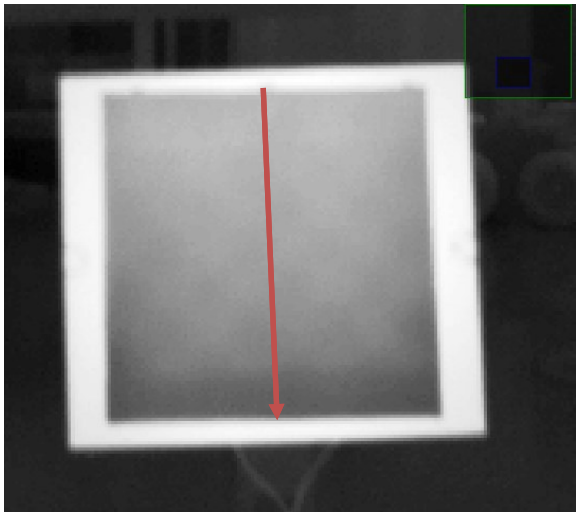

Fig. 5 Obtaining the temperature gradient T' along a vertical line on the objects surface

The detected rectangle will be tested for a temperature gradient by narrowing it down to a line in the middle of the rectangle (see Fig. 5). From this line, n values are taken and stored into the array T.

$$T = [T_0, T_1, T_0, \dots, T_n\ ]$$

Afterwards, the derivation T’ is calculated. If all values of T’[i] ≤ 0 , then a temperature gradient is detected on the surface.

3.3.3 Smoke Detection

Smoke can be detected remotely with a laser scanner. The pointcloud containing the temperature information is used to obtain the position of the detected object (door) in the 3D laserscanner data. The smoke detection approach involves a bounding box around the object (door), where the mean square error *E* of consecutive scans is calculated. In a static case (no smoke), *E* is low. During the presence of smoke, *E* rises due to the dynamic in the 3D lidar data (see Fig. 14).

3.4 High Level Hazard: Hazard Prediction Model

As indicated in Table 1 and Table 2, we classify low-level and high-level hazards. The detection of low level hazards is usually trivial and estimated via thresholding sensor data or running a clustering over tempered 3D point clouds. The prediction of high level hazards is challenging. In section 3.3, we describe how to detect a flashover by going step by step through indications of this effect. A more general approach is the hazard prediction model. Gas, smoke and temperature follow the physical law of diffusion. The diffusion equation is as follows (u= $c_{Propanol}$, $c_{Acetone}$, *LRR*, *T* , *d* = *Diffusion coefficient*):

$$\frac{\partial u}{\partial t} = d\frac{\partial^2 u}{\partial x^2}$$

The values for *u* are stored in the every layer of GDIM. Since the values are distributed in discrete fashion, we need to solve the diffusion equation numerically. For the first numerical derivation, we can apply three different solution (central, forward, backward) depending on the location of boundaries. In case of GDIM, the boundaries are stored in the obstacle map.

$$u' \approx \frac{u(x+\Delta x) - u(x)}{\Delta x} \qquad u' \approx \frac{u(x) - u(x-\Delta x)}{\Delta x} \qquad u' \approx \frac{u(x+\Delta x) - u(x-\Delta x)}{2\Delta x}$$

The central second derivation is as follows:

$$u''(x) \approx \frac{u(x+\Delta x) - 2u(x) + u(x-\Delta x)}{\Delta x^2}$$

The end nodes (cells, which are free, but having an occupied neighbor cell) are determined as follows:

$$u''(x) \approx 2 \cdot \frac{u(x+\Delta x) - u(x)}{\Delta x^2}$$
$$u''(x) \approx -2 \cdot \frac{u(x) - u(x-\Delta x)}{\Delta x^2}$$

Now we can make our numerical solution for the two dimensional case (central version):

$$\frac{U_{i,j}^{t+1} - U_{i,j}^{t}}{\Delta t} = d_x \frac{U_{i+1,j}^{t} - 2U_{i,j}^{t} + U_{i-1,j}^{t}}{\Delta x^2} + d_y \frac{U_{i,j+1}^{t} - 2U_{i,j}^{t} + U_{i,j-1}^{t}}{\Delta y^2}$$

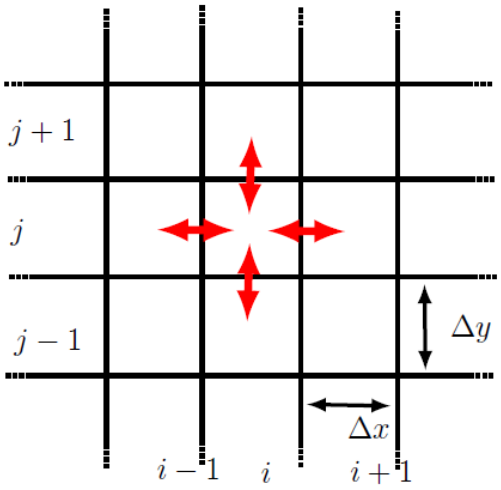

Fig. 6 Every cell of a grid map represents a node for the Finite Difference Method

The hazard_prediction can be started via:

rosrun hazard_prediction predict_map_node

The node subscribes and predicts the following layers of GDIM:

- Temperature layer
- Acetone layer
- Propanol layer
- Smoke layer

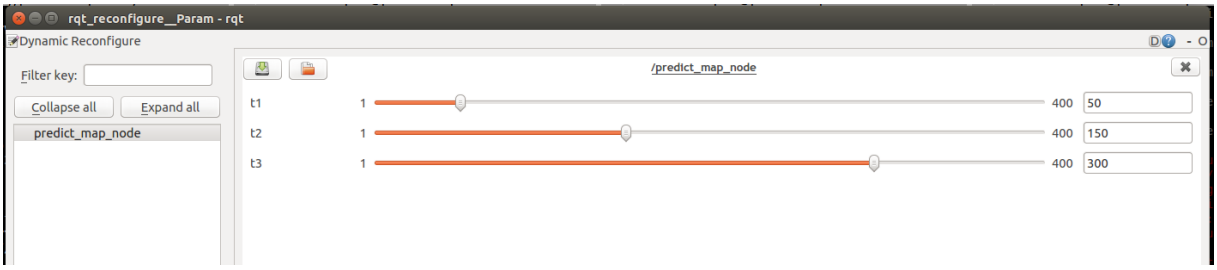

Fig 7. The Finite Difference Method is an iterative algorithm. Through the parameter t1, t2 and t3, the prediction at three points in time can be set.

4. Experiments

4.1 Low Level Hazard: Hotspot Detection in Workshop Environment

A hotspot detection method using LiDAR, radar and thermal vision was implemented and tested. During our experiments, the robot was teleoperated inside a smoky workshop environment. In order to generate smoke, we used a fog machine. Although smoke and fog are physically different, their attenuating influence on light-based range measurement and vision is basically the same. For this reason, instead of creating real smoke, we only use dense fog in our experiments. For evaluating the benefits of the hotspot detection, we placed some electrically heated targets in the workshop. After entering the smoky room, the robot was driven in circles around a metal cupboard a couple of times. The results of the experiments were presented at 2017 SSRR conference [3].

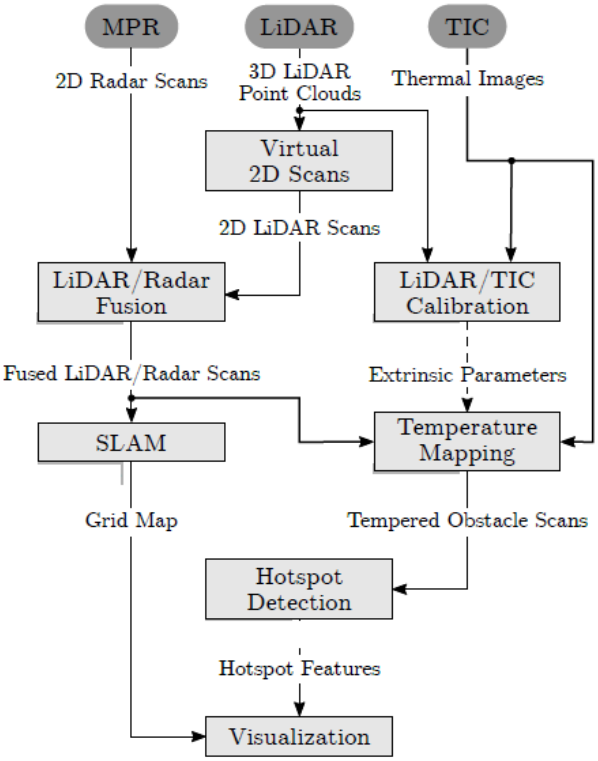

Fig. 8 : Process flow of hot spot detection involves output of T1.3 and T3.2.

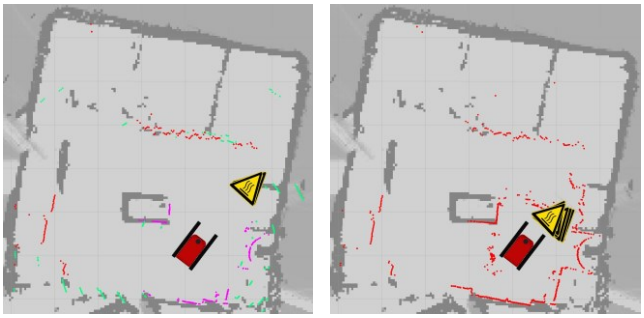

Fig. 9: Hotspots during experimental setup. As can be seen above, only with the integration of all three sensors a hotspot detection can be achieved.

4.2 High Level Hazard: Detection of Pre-Flashover Conditions

To generate a flashover scenario, a heating plate was used as an object. A cardboard was fixed to it and a spacer was used at the bottom to create a temperature gradient. A fog-machine was placed behind the heating plate to generate smoke, meanwhile data from Velodyne and FLIR was recorded (see Fig. 10). The experiment is recorded in a static environment.

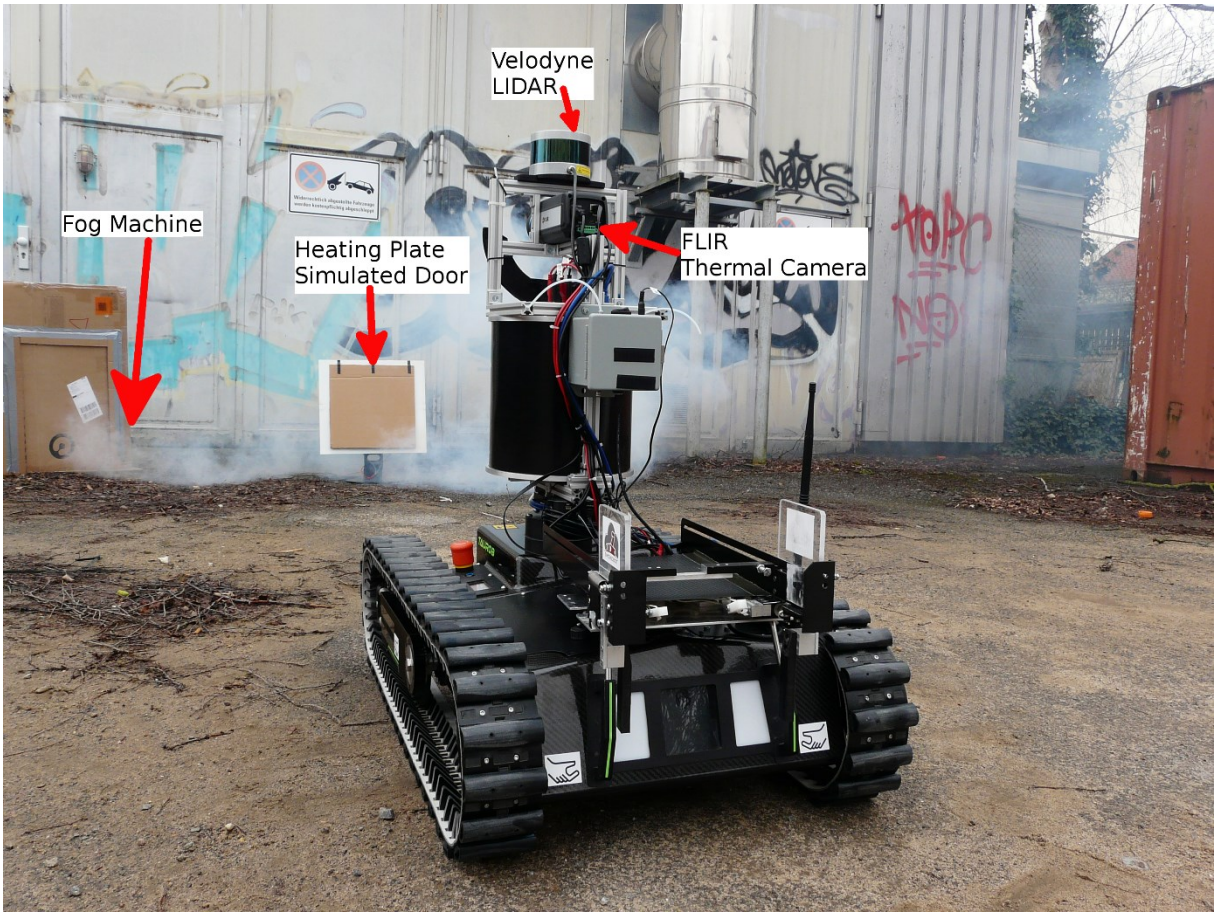

Fig. 10 A flashover is simulated with a heating plate (hot object, as for example door) and a fog-machine (smoke is rising to the roof during flashovers)

During the experiment, it was not possible to generate temperatures around 500°C, as it occurs during a real flashover. Nevertheless, it is possible to distinguish and detect the heating plate, which had a temperature around 35°C. In Firg. 11, it can be seen that the heating plate can be identified. Additionally, the contour of another warm object gets detected but does not fulfill properties of a door (perpendicular contours).

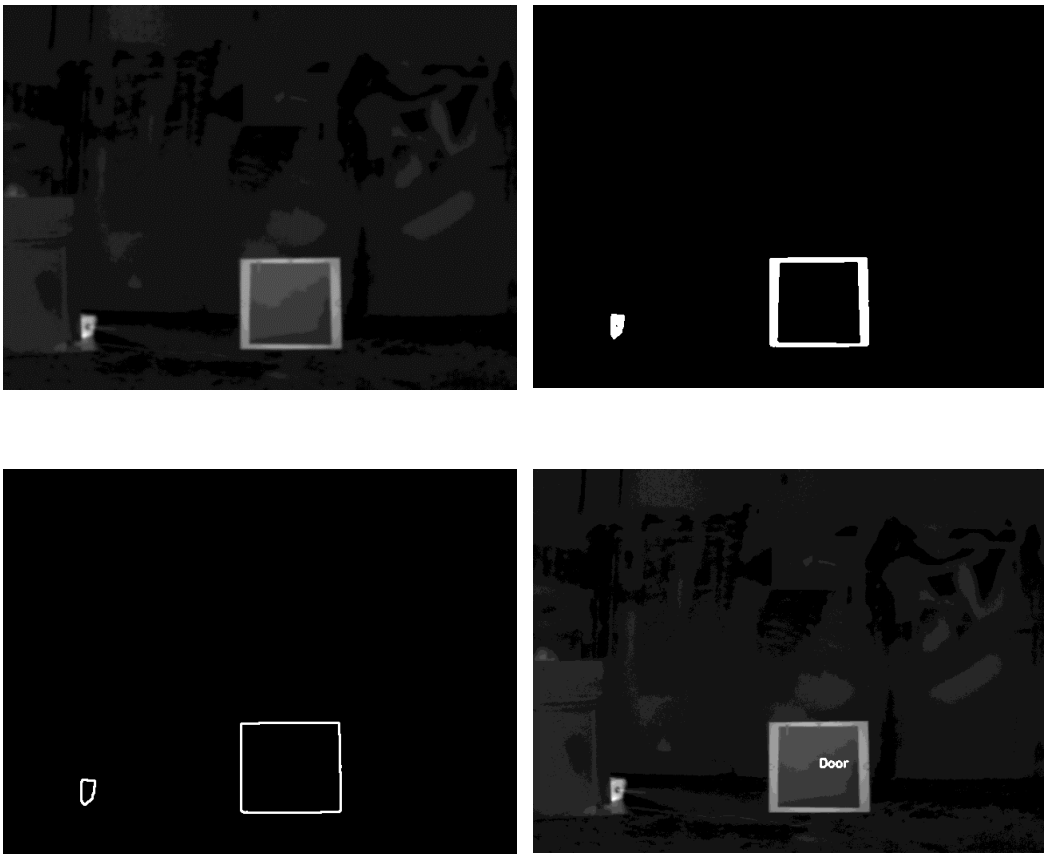

Fig. 11 Identification of rectangular objects

After a likely doorframe was detected in the thermal image, the temperature gradient on the surface is obtained. Fig. 12 represents Temperature along a vertical line on the surface from seven points. The temperatures values represent the cell values in the camera images.

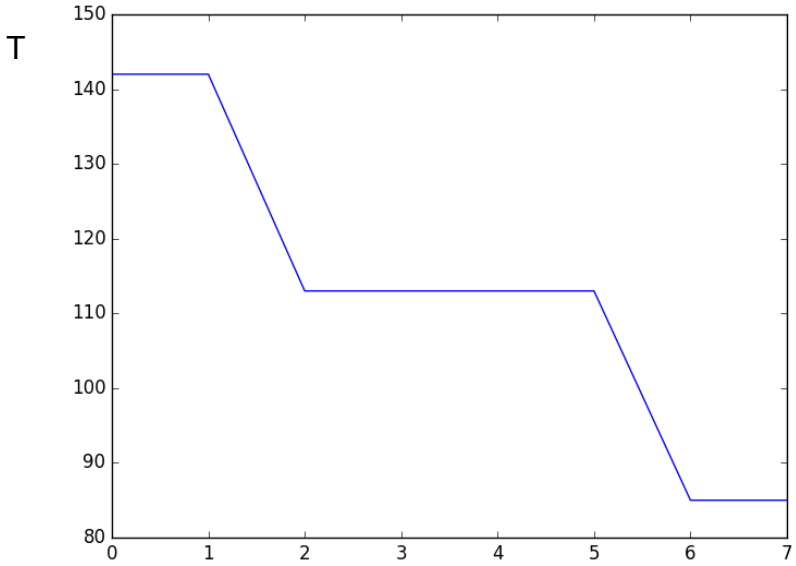

Fig. 12 A temperature gradient is detected on the surface of the object observing eight measurement points on a vertical line.

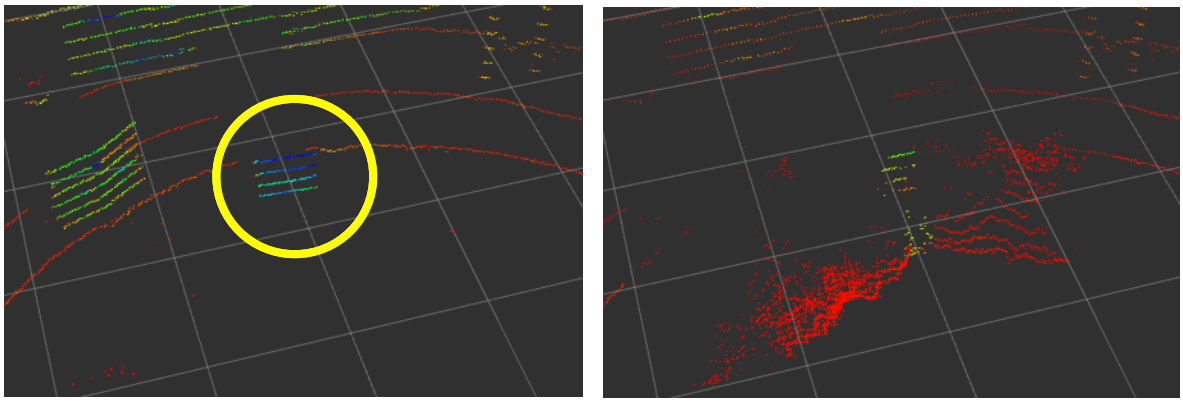

Fig. 13 Left: Object in the 3D Laser data. Right: Due to the smoke 3D laser data around the object gets dynamic.

In Fig. 13, laser data is presented which smoke affects. Consequently, the laser data is more dynamic around the object. A smoke detection is performed using the square mean error of the consecutive laser point inside a bounding box around the object.

$$SQME = \frac{1}{n}\sum_{0}^{n}\sqrt{\left(x_{i,t} - x_{i,t-1}\right)^2 + \left(y_{i,t} - y_{i,t-1}\right)^2 + \left(z_{i,t} - z_{i,t-1}\right)^2}$$

Fig. 14 indicates that the SQME rises if smoke is present.

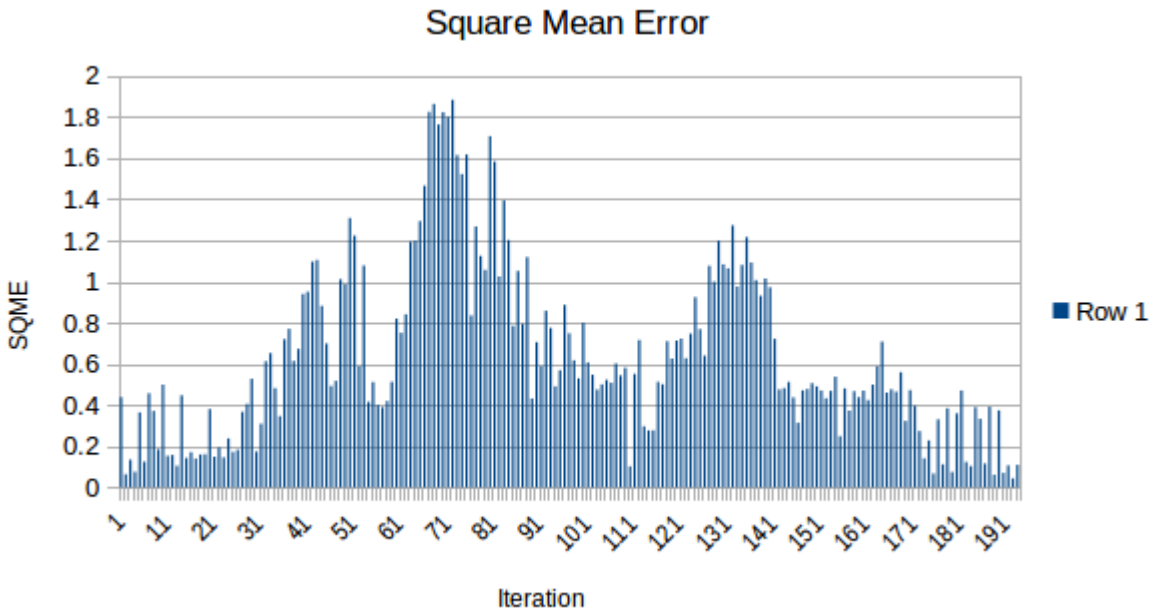

Fig. 14 SQME rises as soon as smoke is present

To sum it up, flashover warning for hot doors can be realized, if a rectangular shape, a temperature gradient and smoke is detected. The experiment proofs that it is possible to detect these indicators in static environments.

The software toolkit is uploaded as hazard_detection_flashover on SmokeBot's git repository.

4.3 High Level Hazard: Hazard Prediction Model

Fig. 15 Experiment at the Brandhaus in Dortmund.

To evaluate the prediction model, we recorded data at the Brandhaus in Dormtund. The temperature layer of GDIM contains information from tempered pointclouds (Task 3.2). Now, the hazard prediction can estimate the distribution of the heat for three points of time, which is indicated in Figure 16. The prediction for other layers of GDIM works likewise.

Fig. 16 Prediction of thermal information to three different time steps. The hot area in the middle of the map is a human.

5. Conclusion

In this document, we described the software toolkit for hazard detection and prediction based on multi-modal perception that is used in the SmokeBot project. In detail, we presented approaches for low-level and high-level hazard prediction, which are visualized through the interface. The detection of flashovers is challenging. In this deliverable, we propose a detection via detecting step-by-step flash over indicators. Furthermore, we present a general model to predict hazards which are caused by temperature, gas and smoke.

References

[1] Peacock, Richard D., et al.: "Defining flashover for fire hazard calculations.", Fire Safety Journal 32.4 (1999): 331-345.

[2] Kunkelmann, Jürgen: “Flashover/Backdraft - Ursachen, Auswirkungen, mögliche Gegenmaßnahmen”, Forschungsbreicht Nr. 130, Forschungsstelle für Brandschutztechnik an der Universität Karlsruhe (2003).

[3] Fritsche, P., Zeise, B., Hemme, P. and Wagner, B.: Fusion of Radar, LiDAR and Thermal Information for Hazard Detection in Low Visibility Environments, Proc. IEEE International Symposium on Safety, Security, and Rescue Robotics (SSRR), pp. 96-101, Shanghai, China, 2017.

[4] http://wiki.ros.org/grid_map (as of 2018/03/16)

Fusion of Radar, LiDAR and Thermal Information for Hazard Detection in Low Visibility Environments

Paul Fritsche, Björn Zeise, Patrick Hemme and Bernardo Wagner
Institute of Systems Engineering - Real Time Systems Group
Leibniz Universität Hannover, Appelstr. 9A, D-30167 Hannover, Germany
fritsche | zeise | hemme | wagner @rts.uni-hannover.de

***Abstract*— Nowadays, mobile robots are widely used to support fire brigades in search and rescue missions. The utilization of those robots – especially under low visibility conditions due to smoke, fog or dust – is limited. Under these circumstances, environmental perception is still a huge challenge. In this work, we present an approach on using LiDAR, radar and thermal imaging in order to detect hazards that are potentially harmful to the robot or firefighters. We show the benefits of fusing LiDAR and radar before projecting temperatures recorded with a thermal imaging camera onto the range scans. Additionally, a hotspot detection method using the tempered range scans is presented. We demonstrate the functionality of our approach by teleoperating a robot through a smoky room.**

I. Introduction

The exploration of disaster environments with severely restricted visibility is dangerous for first responders as they have no knowledge of the current situation and can lose their orientation in the unknown environment. In such dangerous scenarios, a mobile robot can form an overall perspective on the situation and deliver useful information to first responders [1].

Depending on the environment and application, an operator can equip a robot with suitable sensors to detect hazards. An example is given in [2], where the authors used a radiation and a chemical sensor to sense and localize sources of hazards. Optical sensors such as laser scanners and RGB cameras are commonly used for most tasks in mobile robotics and have established themselves as state-of-the-art, but they are severely limited in low visibility environments as shown in Figure 1.

Sensors such as radar scanners and thermal imaging cameras (TICs) can overcome poor visibility conditions but have other limitations in their physical properties. Radar sensors are unable to represent the structure of an environment in the same quality as a LiDAR due to limited range and angular resolution. The temperatures measured by a TIC depend on the material of an object. Additionally, the images can contain reflections which lead to a misinterpretation [3].

Nevertheless, connecting thermal images with structural information brings benefits to the exploration of hazardous environments. One application concept is shown in [4], where distance information from a radar is projected on an infrared image integrated on a small head-mounted display to indicate free space for firefighters. Schoenauer et al. [5] developed a mobile sensor system worn by firemen to construct thermal maps with a depth sensor and a TIC.

Fig. 1: Robot in low visibility environment

In this work, we present a new approach to detecting hazards with a mobile robot in low visibility environments. Therefore, we fuse range data from a LiDAR and a radar sensor to map the unknown environment and merge the fused range data with thermal information. Using the threefold sensor fusion, we realize hazard detection and visual hazard feature representation for first responders.

Initial investigations regarding radar sensors in the field of mobile robots were done at the Australian Centre for Field Robotics in the nineties, where fundamental probabilistic SLAM algorithms in combination with radar were developed [6]. In [7], Adams et al. used radar in the context of robotics for mapping of mines by utilizing a Probability Hypothesis Density (PHD) filter. In opposite to feature-based SLAM approaches, Vivet et al. [8] developed a scan matching method through a Fourier-Mellin transform producing large scale maps. Mapping of indoor environments was performed by Detlefsen [9] and Marck [4].

Research towards extrinsic calibration of a LiDAR and a camera was done in several works. One description of the extrinsic calibration of an RGB camera and a 2D LiDAR is given in [10]. A planar checkerboard pattern is used to find initial guesses for intrinsic and extrinsic parameters. After that, the calibration result is further refined using nonlinear minimization. In works such as [11] and [12], a similar procedure regarding the calibration between a 3D LiDAR and an RGB camera is described. In these approaches, planes are detected in both the laser and camera observations to determine the transformation between the sensor frames. Temperature mapping is a well-known problem not only in the robotics domain. Commonly, a ray tracing algorithm is

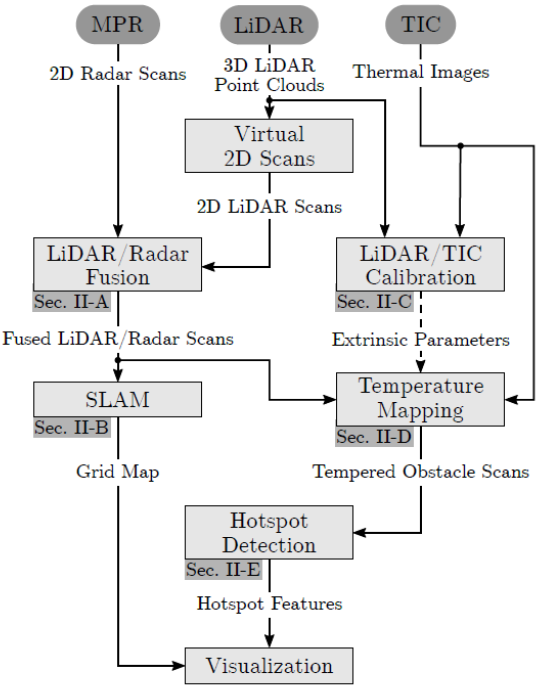

Fig. 2: Overview of the methods presented in this work.

implemented, that calculates the intersections of the laser rays and the camera's image plane. This principle has been applied by e.g. [13], [14] and [15] with different kinds of range sensors.

The remainder of this paper is organized as follows: In Section II, we describe methods improving robot perception in low visibility environments. This includes explanations on LiDAR/radar fusion and SLAM, temperature mapping using fused LiDAR/radar data and thermal images as well as hotspot detection. The evaluation presented in Section III demonstrates the benefits of our approach in low visibility scenarios. In Section IV, we conclude our work and give a short outlook.

II. Methods

In Figure 2, we illustrate the connection of all components contributing to our approach. At first, we fuse radar and LiDAR data to generate 2D obstacle scans that allow environmental perception and map generation under low visibility conditions. After that, we create a tempered obstacle scan by projecting temperature values onto the fused obstacle scan. Therefore, we need to run an extrinsic calibration between LiDAR and TIC after mounting all sensors onto the robot. Using the tempered obstacle scans and the position information of the robot obtained by our SLAM, we visualize hot spots in a user-friendly manner with a 2D map.

A. Fusing LiDAR, Radar and Thermal Information

We fuse a *Velodyne VLP-16* and the *Mechanical Pivoting Radar* (MPR), which was built by the Fraunhofer Institute

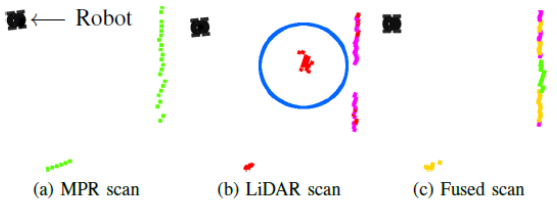

(a) MPR scan (b) LiDAR scan (c) Fused scan

Fig. 3: Our sensor fusion replaces LiDAR points, which are affected by smoke (blue circle), with radar points (green). Yellow points represent R_{Fusion}. Red and magenta points are LiDAR scan points. Magenta represents a line segmentation.

for High Frequency Physics and Radar Techniques for the SmokeBot[1] project. We presented the sensor and first results in [16]. The sensor fusion combines virtual 2D scans [17] with 2D radar scans to generate two fused 2D scans, one for SLAM and the other one for obstacle avoidance. We presented our sensorfusion and SLAM approach in [18]. A fused scan S_{Fusion} contains radar, LiDAR and fused scan points.

$$S_{\text{Fusion}} = [R_{\text{LiDAR}}, R_{\text{Radar}}, R_{\text{Fusion}}, ...] \quad (1)$$

The more aerosols, which disturb the LiDAR, an environment contains, the more radar scan points are in the fused scan S_{Fusion}.

Figure 3 shows results from first experiments, where we created low visibility conditions with a fog machine [16]. We observed two effects related to aerosols using the LiDAR. First, aerosols can lead to a detection, which is visualized with a blue circle in Figure 3b. We call this effect *Type I*.

If the LiDAR is very close or inside an aerosol cloud, then the laser pulses get absorbed and no interpretable echoes are received. Therefore, the sensor is interpreting it as an infinite measurement (inf). We call this effect *Type II*.

There are several techniques for SLAM. Mainly, they can be divided into filter-based and optimization-based approaches. We presented a more detailed description of our SLAM approach in [18]. Our SLAM is based on ICP registration between the fused scan S_{Fusion} and a grid map. The data association is based on Euclidean distances and the distinction according to the fusion cases.

Additionally, our data association takes into account if a grid cell has been observed from the current robot position before by distinguishing eight viewing angles for every cell. Hence, we store in each cell the direction from where it has been seen.

After data association, we calculate the transformation between the fused scan and the grid map, which represents the measurement inside a Kalman filter. The prediction of the Kalman filter can be based on the odometry and the motion model of the robot or a linear motion model if no odometry is available.

The hotspot detection method presented in Section II-C relies on a robust temperature mapping approach. During

[1] http://www.smokebot.eu/

temperature mapping, thermal images recorded by the TIC are projected onto range scan points. Those range scans can be pure LiDAR, pure radar or a combination of both. Since no explicit calibration between the radar scanner and the TIC is performed in this work, we assume the scans (regardless of their origin) to be provided with respect to the LiDAR coordinate frame. In order to calibrate the LiDAR and the TIC, we use a method that we presented in one of our previous works [19]. It is based on minimization of point-to-plane distances as described in [10].

B. 2D Tempered Obstacle Scans

A homogeneous, fused LiDAR/radar point ${}_{(L)}\tilde{\boldsymbol{x}}_{LR} = ({}_{(L)}\tilde{x}_{LR}, {}_{(L)}\tilde{y}_{LR}, {}_{(L)}\tilde{z}_{LR}, 1)^T$ with respect to $\boldsymbol{L}$, which is part of a fused scan S_{Fusion}, can be projected onto the TIC's image plane using the following expression:

$$\tilde{w} \begin{pmatrix} u \\ v \\ 1 \end{pmatrix} = \boldsymbol{K} \left[\boldsymbol{R}_{(LC)} \,|\, \boldsymbol{t}_{(LC)} \right] {}_{(L)}\tilde{\boldsymbol{x}}_{LR}, \tag{2}$$

with the priorly known intrinsic camera matrix $\boldsymbol{K}$, image coordinates $(u, v)^T$, scaling factor $\tilde{w}$ and extrinsic transformation matrix $\left[\boldsymbol{R}_{(LC)} \,|\, \boldsymbol{t}_{(LC)} \right]$. Since Equation 2 depicts a complete 3D-to-2D projection, the projection of a 2D fused LiDAR/radar point, i.e. a 3D point with a constant height ${}_{(L)}z_{LR}$, is straightforward. By assigning a temperature value to every individual point, a tempered obstacle scan S_{Temp} is being constructed.

When generating 2D fused LiDAR/radar scans S_{Fusion}, all obstacles relevant to the robot are taken into account. The same behavior is pursued during temperature mapping of a point ${}_{(L)}\boldsymbol{x}_{LR} = ({}_{(L)}x_{LR}, {}_{(L)}y_{LR}, {}_{(L)}z_{LR})^T$: Using the robot's dimensions, minimum and maximum heights z_{min} and z_{max}, respectively, are determined (see also Figure 4). With the help of those limits, two additional 3D points using z_{min} and z_{max} instead of ${}_{(L)}z_{LR}$ are projected onto the TIC's image plane. Along the vertical line between the resulting points ${}_{(I)}\boldsymbol{x}_{LR,\text{min}}$ and ${}_{(I)}\boldsymbol{x}_{LR,\text{max}}$, all corresponding temperatures in the thermal images are investigated. Only the highest temperature is integrated into the tempered obstacle scan.

C. Hotspot Detection

The tempered obstacle scans obtained from temperature mapping are used to detect hotspots. For this purpose, the scan points are clustered according to their temperatures. If a cluster reaches a predefined size and consists of points with temperatures greater than a specific threshold, we generate a hotspot feature. Besides the recording time stamp and the coordinate frame to which the hotspot's location is related, a hotspot feature contains the following information:

- Hotspot's location
- Variance of location
- Average temperature of all points belonging to the hotspot
- Variance of average temperature

Algorithm 1: Hotspot detection

Input : $S_{\text{Temp}} = \{\boldsymbol{x}_{\text{Temp}}^{(k)}\}$ with $k \in \{1, 2, ..., K\}$
T_{max}
Output: Array $\boldsymbol{h}$ containing hotspot features $h^{(l)}$ with $l \in \{1, 2, ..., L\}$

```
for k ← 1 to K do
    H ← InitializePointCloud()
    if T^(k) > T_max then
        Add x_Temp^(k) to H
    end
end
C ← EuclideanClusterExtraction(H)
L ← sizeof(C)
h ← InitializeArray()
for l ← 1 to L do
    x̄_Temp^(l) ← CalcMeans(C^(l))
    Var(C^(l)) ← CalcVars(C^(l), x̄_Temp^(l))
    NPnts ← sizeof(C^(l))
    h^(l) ← HotspotGen(x̄_Temp^(l), Var(C^(l)), NPnts)
    Add h^(l) to h
end
```

- Size of hotspot cluster (number of points forming the hotspot)

Algorithm 1 presents the hotspot detection procedure using a tempered obstacle scan S_{Temp} as input. A scan contains K tempered scan points $\boldsymbol{x}_{\text{Temp}}^{(k)} = \left(x^{(k)}, y^{(k)}, z^{(k)}, T^{(k)}\right)^T$. Every individual point is defined by 3D point coordinates ($x^{(k)}$, $y^{(k)}$ and $z^{(k)}$) as well as a temperature value $T^{(k)}$. Additionally, a temperature threshold T_{max} has to be provided. The result of this procedure is a vector $\boldsymbol{h}$ containing all detected hotspots including their properties mentioned above.

III. Evaluation

The following sections describe the experimental setup that was used to evaluated the presented methods. The focus was on the evaluation of the benefits of LiDAR/radar scan fusion and hotspot detection.

A. Experimental Setup

Figure 5 depicts the mobile robot platform (*taurob tracker*) that was used for evaluation. Besides several other sensors, the robot is equipped with a 3D LiDAR sensor, a 2D radar scanner and a thermal imaging camera.

The LiDAR used in the experiments is a *Velodyne VLP-16*. It provides 360° scans consisting of 16 horizontal scan lines. It is able to take measurements of up to 100 m and works at a rate of 10 Hz. The 2D radar scanner is the *MPR*, which provides range measurements at a maximum rate of 2.5 Hz. The measurement range is between 0.2 m and 15 m. The TIC in our experimental setup is a *FLIR A655sc* with a spatial

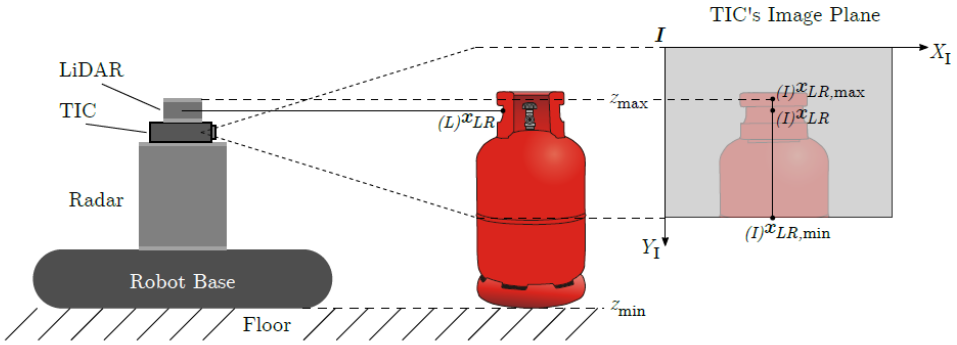

Fig. 4: Side view illustration of the robot platform and the sensor stack looking at a potential heat source: Using the robot's dimensions and corresponding vertical limits z_{min} and z_{max}, an imaginary line along those boundary points can be created in the thermal image (depicted on the right-hand side). Investigating all temperatures on the line between ${}_{(I)}x_{LR,min}$ and ${}_{(I)}x_{LR,max}$, only the highest one is integrated into the tempered obstacle scan S_{Temp}. If the projected pendants of z_{min} and z_{max} lie outside of the image, the limits are accordingly adapted (as is the case with ${}_{(I)}x_{LR,min}$).

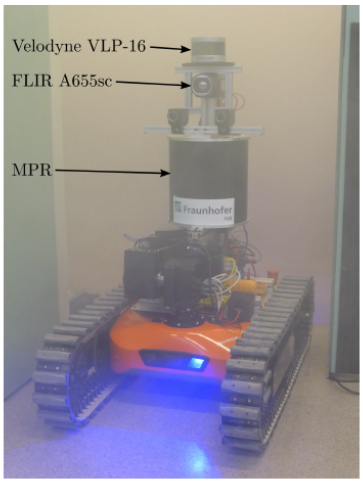

Fig. 5: Sensor setup

Fig. 6: Workshop environment with fog machine (left) and heat targets (marked with the green circles).

resolution of 640 × 480 pixels. It works in the spectral range between 7.5 µm and 14 µm. The camera's FOV is 45° × 34°.

During our experiments, the robot was teleoperated inside a smoky workshop environment. In order to generate smoke, we used a fog machine. Although smoke and fog are physically different, their attenuating influence on light-based range measurement and vision is basically the same. For this reason, instead of creating real smoke, we only use dense fog in our experiments. For evaluating the benefits of the hotspot detection, we placed some electrically heated targets in the workshop (see Figure 6). After entering the smoky room, the robot was driven in circles around a metal cupboard a couple of times.

B. Scan Fusion

The sensor fusion between LiDAR and MPR provides two scans. One scan is used for SLAM in order to build a map. The MPR has a lower scan quality, which affects the mapping as well. In combination with the virtual 2D scan method, our sensor fusion creates scans which contain as less as possible pure radar points. Only if no suitable LiDAR points are available, then radar is used for SLAM. We show this case in [18]. The other scan of the sensor fusion is used for obstacle avoidance and hazard detection. As can be seen in Figure 9b, sometimes no suitable LiDAR points to describe an obstacle can be found. In this case, effect *Type I* occurs in the near scan field and our sensor fusion replaces the LiDAR points with radar points. The composition of the scans for SLAM and hazard detection during the whole test run is presented in Figure 7.

C. Hotspot Detection

Figure 8 shows the functionality of the map creation using our SLAM as well as the generation of tempered obstacle scans using fused LiDAR/radar scans and thermal images as input (see Section II-B). Comparing Figures 8a and 8b, it can be seen that the method for filtering the maximum

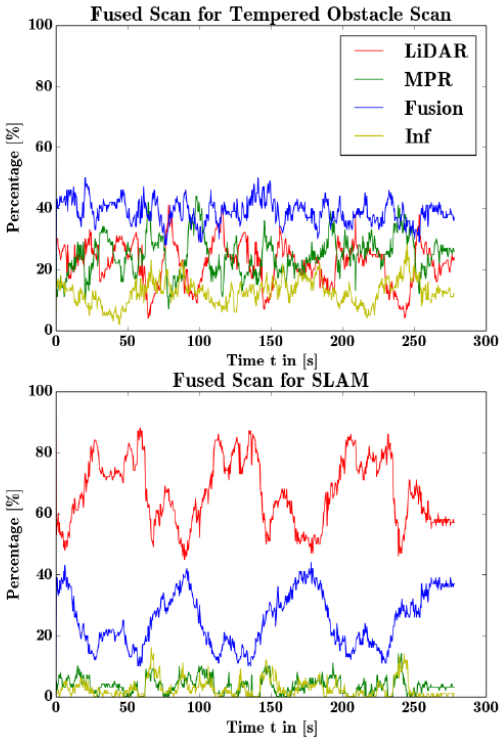

Fig. 7: Composition of the fused scans for SLAM and obstacle avoidance during the experiment.

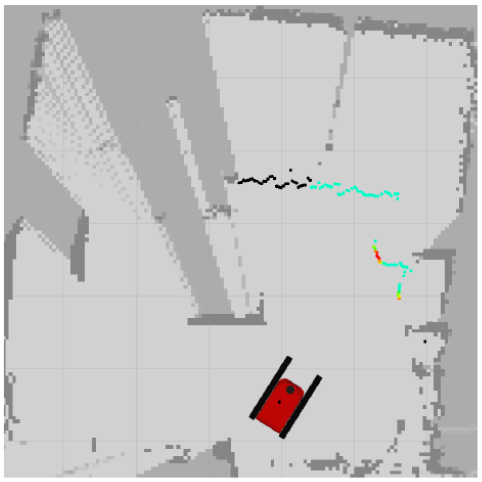

(a) Map with tempered obstacle scan

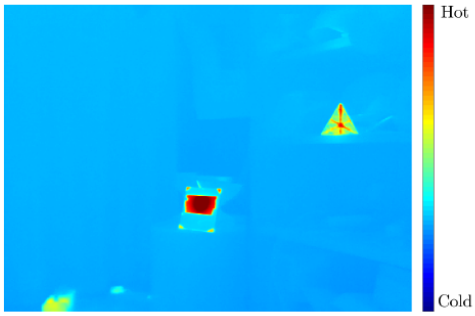

(b) Corresponding thermal image

Fig. 8: Top-down view of the workshop environment: (a) Several artificial hotspots have been placed in the room in order to show the functionality of the tempered obstacle scans, which are integrated into the 2D grid map generated using SLAM; (b) corresponding thermal image from the robot's point of view.

temperatures from the thermal images before integrating them into the tempered obstacle scans works well: Both heat targets displayed in the thermal image can also be found in the tempered obstacle scan.

Since the room was filled with smoke during our experiment, the pure laser scans contain scattered points in the space between the robot and the actual obstacles. Comparing Figures 9a and 9b, the benefit of using fused LiDAR/radar scans for hotspot detection becomes clear: If the hotspot detection would have been performed on the pure laser scans (as depicted in Figure 9b), wrong hotspot features would be generated. In Figure 9a, where we used the fused LiDAR/radar scans during temperature mapping, the hotspot detection works well.

IV. Conclusion and Future Work

In this work, we presented methods improving mobile robot perception in smoky environments. We fused both laser and radar scans exploiting the individual sensors' advantages under different visibility conditions. The fused LiDAR/radar scans serve as input for a SLAM procedure that is able to generate a grid map representation of the environment. Additionally, we created tempered obstacle scans using fused LiDAR/radar data in combination with thermal images. With the help of those tempered scans, we were able to detect hotspot hazards.

During evaluation, we teleoperated a robot equipped with aforementioned sensors through a smoky workshop environment. We demonstrated that – by using fused LiDAR/radar information – on the one hand a robust grid map can be generated, and on the other hand hotspots can reliably be detected. The comparison between the hotspot detection relying on fused data and an approach using pure laser scan data as input showed obvious advantages on the side of the former one.

Future work will focus on the integration of the detected hotspot features into a specific map layer of the environmental representation. This will be done in a probabilistic way in order to cope with measurement uncertainties and corresponding misdetections.

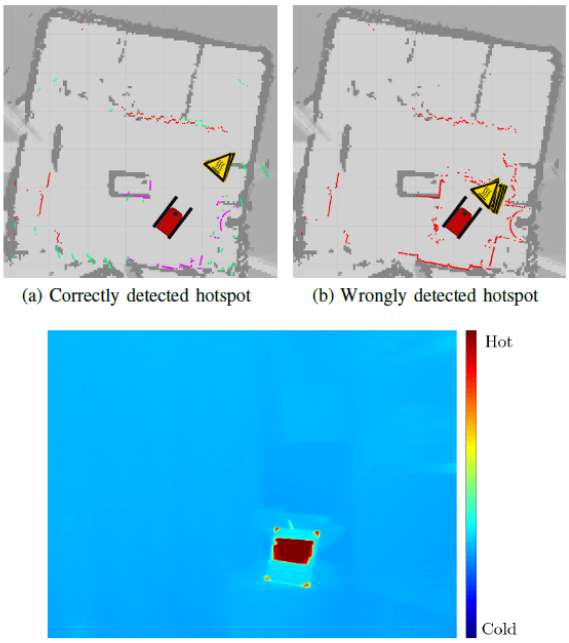

(a) Correctly detected hotspot (b) Wrongly detected hotspot

(c) Corresponding thermal image

Fig. 9: Top-down view of the workshop environment: (a) 2D grid map with fused LiDAR/radar scan and correctly detected hotspot; (b) wrongly detected hotspot due to usage of pure laser scans as input of temperature mapping; (c) corresponding thermal image from the robot's point of view.

ACKNOWLEDGMENT

This work has partly been supported within H2020-ICT by the European Commission under grant agreement number 645101 (SmokeBot).

REFERENCES

[1] R. R. Murphy, "Trial by fire [rescue robots]," *IEEE Robot. Automat. Mag.*, vol. 11, no. 3, pp. 50–61, 2004.

[2] C. W. Neilsen, D. I. Gertman, D. J. Bruemmer, R. S. Hartley, and M. C. Walton, "Evaluating robot technologies as tools to explore radiological and other hazardous environments," in *Proc. American Nuclear Society Emergency Planning and Response, and Robotics and Security Systems Joint Topical Meeting*, 2008.

[3] B. Zeise, S. P. Kleinschmidt, and B. Wagner, "Improving the interpretation of thermal images with the aid of emissivity's angular dependency," in *Proc. 2015 IEEE Int. Symp. Safety, Security, and Rescue Robotics*. IEEE, 2015, pp. 1–8.

[4] J. Marck, A. Mohamoud, E. v.d. Houwen, and R. van Heijster, "Indoor radar SLAM a radar application for vision and GPS denied environments," in *2013 European Radar Conf. (EuRAD)*, 2013, pp. 471–474.

[5] C. Schönauer, E. Vonach, G. Gerstweiler, and H. Kaufmann, "3D building reconstruction and thermal mapping in fire brigade operations," in *Proc. 4th Augmented Human Int. Conf.* ACM, 2013, pp. 202–205.

[6] S. Clark and G. Dissanayake, "Simultaneous localisation and map building using millimetre wave radar to extract natural features," in *Proc. 1999 IEEE Int. Conf. Robotics and Automation*, vol. 2, 1999, pp. 1316–1321.

[7] M. Adams and E. Jose, *Robotic navigation and mapping with radar*. Artech House, 2012.

[8] D. Vivet, P. Checchin, and R. Chapuis, "Localization and mapping using only a rotating FMCW radar sensor," *Sensors 13, no. 4*, pp. 4527–4552, 2013.

[9] M. Lange and J. Detlefsen, "94 GHz 3D-imaging radar for sensor-based locomotion," in *IEEE MTT-S International Microwave Symposium Digest*, vol. 3, 1989, pp. 1091–1094.

[10] Q. Zhang and R. Pless, "Extrinsic calibration of a camera and laser range finder (improves camera calibration)," in *Proc. IEEE/RSJ Int. Conf. Intelligent Robots and Systems*, vol. 3. IEEE, 2004, pp. 2301–2306.

[11] G. Pandey, J. McBride, S. Savarese, and R. Eustice, "Extrinsic calibration of a 3D laser scanner and an omnidirectional camera," *Proc. 7th IFAC Symp. Intelligent Autonomous Vehicles*, vol. 43, no. 16, pp. 336 – 341, 2010.

[12] X. Gong, Y. Lin, and J. Liu, "3D LIDAR-camera extrinsic calibration using an arbitrary trihedron," *Sensors*, vol. 13, no. 2, pp. 1902–1918, 2013.

[13] M. I. Alba, L. Barazzetti, M. Scaioni, E. Rosina, and M. Previtali, "Mapping infrared data on terrestrial laser scanning 3D models of buildings," *Remote Sensing*, vol. 3, no. 9, pp. 1847–1870, 2011.

[14] D. Borrmann, J. Elseberg, and A. Nüchter, "Thermal 3D mapping of building façades," in *Intelligent Autonomous Systems 12*, 1st ed., ser. Advances in Intelligent Systems and Computing, S. Lee, H. Cho, K.-J. Yoon, and J. Lee, Eds. Berlin et al.: Springer, 2013, no. 193, pp. 173–182.

[15] S. Vidas, P. Moghadam, and M. Bosse, "3D thermal mapping of building interiors using an RGB-D and thermal camera," in *Proc. IEEE Int. Conf. Robotics and Automation*. IEEE, 2013, pp. 2311–2318.

[16] P. Fritsche, S. Kueppers, G. Briese, and B. Wagner, "Radar and LiDAR sensorfusion in low visibility environments," in *Proc. 13th Int. Conf. Informatics, Automation and Robotics*, vol. 2. Scitepress, 2016, pp. 30–36.

[17] O. Wulf, K. O. Arras, H. I. Christensen, and B. Wagner, "2D mapping of cluttered indoor environments by means of 3D perception," in *Proc. Int. Conf. Robotics and Automation*, vol. 4, 2004, pp. 4204–4209.

[18] P. Fritsche and B. Wagner, "Modeling structure and aerosol concentration with fused radar and LiDAR data in environments with changing visibility," in *IEEE/RSJ Int.Conf. Intelligent Robots and Systems*, 2017, in Press.

[19] B. Zeise and B. Wagner, "Temperature correction and reflection removal in thermal images using 3D temperature mapping," in *Proc. 13th Int. Conf. Informatics in Control, Automation and Robotics*, vol. 2. Scitepress, 2016, pp. 158–165.